Kinetics of Nanobubble Generation Around Overheated Nanoparticles

Julien Lombard, Thierry Biben, and Samy Merabia*
Institut Lumière Matière, UMR5306 Université Lyon 1-CNRS, Université de Lyon, 69622 Villeurbanne cedex, France
(Received 4 July 2013; revised manuscript received 12 February 2014; published 12 March 2014)

We report on the formation and growth of nanobubbles around laser-heated gold nanoparticles in water. Using a hydrodynamic free-energy model, we show that the temporal evolution of the nanobubble radius is asymmetrical: the expansion is found to be adiabatic, while the collapse is best described by an isothermal evolution. We unveil the critical role of the thermal boundary resistance in the kinetics of formation of the nanobubbles: close to the vapor production threshold, nanobubble generation is very long, yielding optimal conditions for laser-energy conversion. Furthermore, the long appearance times allow nanoparticle melting before the onset of vaporization.

DOI: 10.1103/PhysRevLett.112.105701 PACS numbers: 64.70.fh, 05.70.Ln, 05.70.Np

Introduction.—Gold nanoparticles (GNPs) are very promising tools for cancer diagnosis and possible therapy [1]. Owing to their unique biochemical compatibility, GNPs have demonstrated their ability to accumulate in diseased areas. In addition to cell discrimination, GNPs are very efficient absorbers of visible light [2]. These specific interactions open the way to induce localized damage "with a switch" as GNPs within a laser beam may be heated by several tenths of a Kelvin, leading to a large temperature change in the surrounding medium that could allow for tumor destruction [3]. In particular, if the laser energy is sufficiently high, the surrounding medium may undergo boiling, resulting in the formation of transient vapor nanobubbles [4,5]. With sizes up to several microns and a lifetime of hundredths of a nanosecond, these nanobubbles appear to be a promising tool to manipulate and destroy the cellular structure, eventually leading to cell death [6].

Experimental observations on nanobubble formation have mainly focused on the generation threshold and its relation with the crossing of the fluid spinodal [7,8]. Yet the kinetics of formation of the nanobubbles has so far never been characterized. In this Letter, we address this issue using a hydrodynamic free-energy model. Our results show a sharp slowing down of the vaporization process close to the nanobubble generation threshold. We discuss two important implications: (i) the existence of an optimum in efficiency, and (ii) the possibility of nanoparticles melting before vaporization occurs. Experimental results are reinterpreted in light of these new insights.

Model.—We resort to and extend a hydrodynamic model based on a free energy density which has been successfully applied to address interfacial heat transport and boiling at the nanoscale [9,10]. We solve the hydrodynamic equations to describe the dynamics of the fluid around the nanoparticle,

$$\frac{\partial \rho}{\partial t} + \nabla \cdot (\rho \mathbf{v}) = 0, \tag{1}$$

$$m\rho\left(\frac{\partial \mathbf{v}}{\partial t} + \mathbf{v}\cdot\nabla\mathbf{v}\right) = -\nabla\cdot(\mathbf{P}-\mathbf{D}),$$

$$m\rho c_v\left(\frac{\partial T}{\partial t} + \mathbf{v}\cdot\nabla T\right) = -l\nabla\cdot\mathbf{v} + \nabla\cdot(\lambda\nabla T) + \mathbf{D}:\nabla v,$$

where ρ, $\mathbf{v}$, T, and m stand, respectively, for the number density, the velocity field, the temperature, and the mass of a fluid molecule; c_v, l, λ, $\mathbf{D}$, and $\mathbf{P}$ are the fluid specific heat, Clapeyron coefficient, dissipative stress tensor, and pressure tensor, respectively, which are dependent on the local state of the fluid through a van der Waals free energy density [11]. The thermophysical and transport coefficients of water are summarized in Table I, together with the water-vapor surface tension γ.

For the metal nanoparticle, the temperature T_{np} is assumed to be uniform—a reasonable hypothesis owing to the large conductivity of the metal. Its temporal evolution is described by

$$V_{\mathrm{np}}C_{\mathrm{np}}\frac{dT_{\mathrm{np}}}{dt} = F\sigma_{\mathrm{np}}\frac{\Pi(t/t_p)}{t_p} - S_{\mathrm{np}}\phi,$$

$$\phi = \max(G(T_{\mathrm{np}} - T_{\mathrm{surface}}), \phi_b), \tag{2}$$

where S_{np}, V_{np} are the nanoparticle surface and volume, respectively, and $C_{\mathrm{np}} = 2500\ \mathrm{kJ\,m^{-3}\,K^{-1}}$ is the metal's specific heat. The laser interaction is described by the size-dependent GNP absorption cross section σ_{np} as given in Ref. [7], the fluence of the laser pulse F, and the gate function $\Pi(t/t_p) = 1$ if $0 < t < t_p$, 0 otherwise, where the laser duration is set here to $t_p = 7$ ps [12,13]. The water-GNP interaction is described by ϕ which compares a conductive heat flux when the fluid in contact with the GNP is in the liquid state, to a ballistic heat flux ϕ_b [11] when the fluid locally vaporizes. The conductance G was set to $140\ \mathrm{MW\,m^{-2}\,K^{-1}}$, corresponding to a water/GNP contact angle $\theta = 50°$ [14,15].

TABLE I. Thermophysical parameters in the liquid (top row) and in the vapor (bottom row) at 297 K in SI units unless specified.

Density[a]	C_v[b]	λ	η	l	γ
997.10	4.13	0.606	8.98×10^{-4}	5.4×10^{8}	72.0×10^{-3}
2.22×10^{-2}	1.44	0.019	9.9×10^{-6}	6881	

[a] kg/m^3.
[b] kJ/kgK.

Results.—The thermomechanical evolution of the fluid after heating the GNP has been simulated for different laser fluences F and radii R. If the fluence is high enough, we observe after a delay the formation of a nanobubble around the GNP, as represented in Fig. 1. A nanobubble is said to be formed when locally the fluid density is smaller than the critical fluid density.

Figure 2 displays the typical evolution of the nanobubble radius after laser heating, for different laser fluences. Nanobubbles are observed when the laser fluence exceeds a threshold, which is found to correspond to spinodal crossing in the fluid, at a distance $x \simeq 2$ nm from the GNP surface. For fluences F just above the threshold, only transient vapor shells are visible, as is the case for the lowest energy pulse reported in Fig. 2; stronger pulses lead to larger sizes and lifetimes with the possible formation of a subsequent secondary nanobubble. Remarkably the dynamics of the nanobubbles is asymmetrical: the growth is faster than the collapse. To understand this asymmetry, we have compared the simulation results to the solution of the Rayleigh-Plesset equation classically used to describe cavitation phenomena,

$$m\rho_{\mathrm{liq}}\left(R_b\ddot{R}_b + \frac{3}{2}\dot{R}_b^2\right) = P_i(t) - P_e(t) - 2\frac{\gamma}{R_b} - 4\eta\frac{\dot{R}_b}{R_b},$$
$$P_i(t) = P_i^{\max}\left(\frac{R_{b,\max}^3 - R^3}{R_b^3(t) - R^3}\right)^{\zeta}, \qquad (3)$$

where R_b is the bubble radius, P_i and P_e are the internal and external pressures, respectively, and γ is the fluid surface tension. $m\rho_{\mathrm{liq}}$ is the mass density of the liquid far from the nanoparticle given in Table I.

To determine the unknown internal pressure, we have assumed that the pressure inside the bubble is well described by Eq. (3), where $P_i^{\max}$ is the pressure measured in the simulations inside the bubble when its radius is maximal ($R_b = R_{b,\max}$) and the exponent ζ is a fitting parameter. Further details can be found in Ref. [11]. From this fitting procedure, it turned out that it was impossible to describe the nanobubble dynamics with a single exponent ζ, and we resorted to considering two values of ζ: $\zeta = 5/3$ describes well the bubble expansion, while $\zeta = 1$ allows us to match the collapse dynamics (see Fig. 2). The initial growth of the nanobubble is consistent with an adiabatic process, where thermal conduction has not been allowed to set in. When the nanobubble reaches its maximal radius, thermal loss becomes operative and the collapse is nearly isothermal. This difference in the nature of the dynamics explains the asymmetry of the bubble evolution.

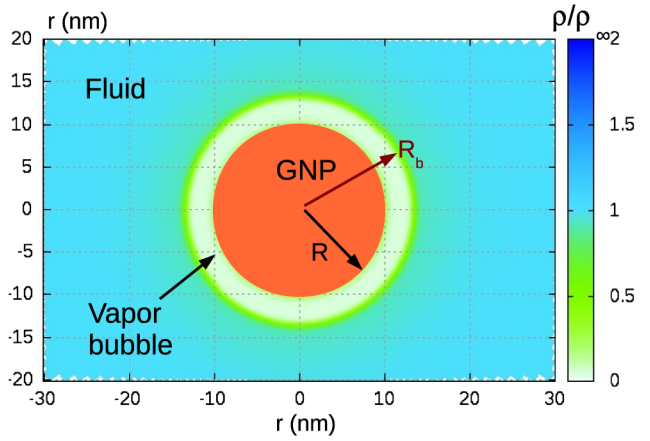

FIG. 1 (color online). Sketch of the system simulated: a gold nanoparticle heated by a femtosecond laser pulse, surrounded by water and a vapor nanobubble at its maximum radius, 118 ps after the beginning of the pulse. Here $R = 10$ nm and $F = 162$ J m^{-2}.

Kinetics of the nanobubble formation.—Nanobubbles form in our simulations when the laser fluence exceeds a threshold which depends on the nanoparticle size. This latter threshold has been found to be consistent with spinodal crossing in the fluid at a distance $x \simeq 2$ nm from the nanoparticle surface. This length scale accounts for the GNP/water wetting interaction and the finite intrinsic thickness of the liquid-vapor interface formed in a strong

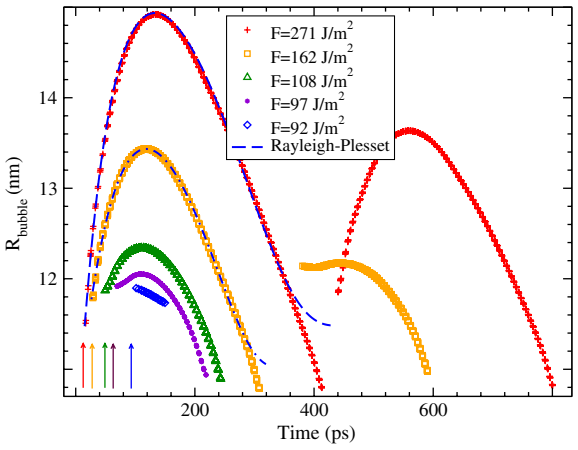

FIG. 2 (color online). Temporal evolution of the nanobubble radius around a 10 nm GNP for different pulse fluences (the higher fluence giving the larger bubbles). A secondary bubble is observed for strong pulses. The arrows indicate the appearance time for each simulation. The dashed lines are the best fits using the Rayleigh-Plesset equation (3).

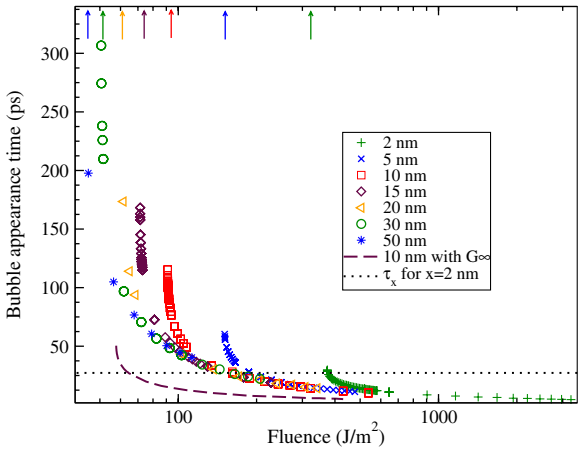

FIG. 3 (color online). Nanobubble appearance time t_{vap} measured in the thermohydrodynamic simulations as a function of the laser fluence for particle radii varying from 2 nm to 50 nm. The horizontal dotted line shows the characteristic diffusion time τ_x over the length scale $x = 2$ nm relevant to spinodal crossing. The dashed line is a simulation result using a particle of radius 10 nm and an infinite conductance $G_\infty \gg G$. The arrows on the top indicate the position of the threshold fluence for bubble appearance.

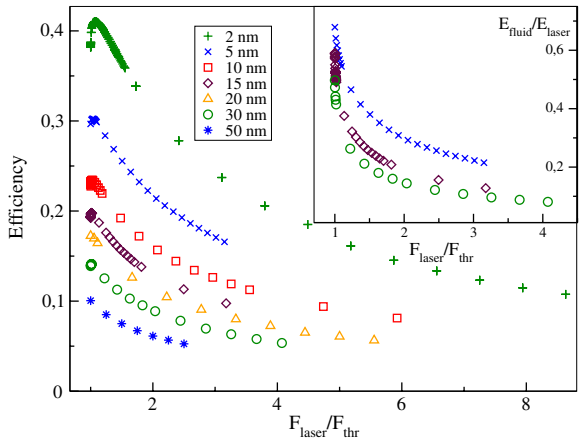

FIG. 4 (color online). Efficiency of the energy conversion $\Gamma = E_{2\mathrm{nm}}/E_{\mathrm{laser}}$ as a function of the laser fluence normalized by the threshold fluence, for particle radii varying from 2 nm to 50 nm. The inset shows the total energy transferred to the fluid E_{fluid} before the bubble appears.

temperature gradient. Remarkably, we have found that the kinetics of vaporization may be very slow, depending on the distance to the threshold fluence. The long vaporization times are illustrated in Fig. 3 for different nanoparticle sizes.

The vaporization time is found to be a strongly decreasing function of the fluence, especially in the vicinity of the threshold fluence F_{thr}. At the threshold, the appearance time is several times larger than the typical diffusion time $\tau_x = x^2 m\rho_{\mathrm{liq}} C_v/\lambda$ over a distance $x = 2$ nm relevant to spinodal crossing. This slow kinetics is to a large extent explained by the existence of a finite thermal boundary resistance at the interface between the GNP and the fluid. Indeed, if the interface is made perfectly conductive and has a vanishing boundary resistance, the vaporization kinetics is several times faster, as shown in Fig. 3. In this ideal case, the bubble appearance time is divided by a factor of 10 in the vicinity of the bubble threshold, amounting to times comparable with τ_x. This demonstrates the prominent role of the Kapitza resistance in the kinetics of formation of the nanobubbles, which severely delays the energy transfer from the GNP to the fluid, thus preventing rapid heating of the fluid in the vicinity of the particle and possible vaporization. As we now discuss, the existence of long appearance times have far-reaching consequences as they directly control the efficiency of the energy conversion and can result in the melting of the nanoparticle before vaporization.

Efficiency.—It is highly instructive to estimate the efficiency of the energy conversion $\Gamma = E_{2\mathrm{nm}}/E_{\mathrm{laser}}$ for the process leading to vaporization. This latter quantity may be defined as the ratio of the energy $E_{2\mathrm{nm}}$ stored in a 2 nm area around the particle before vaporization over the energy supplied by the femtosecond laser pulse $E_{\mathrm{laser}} = F\sigma_{\mathrm{np}}$. Figure 4 displays the efficiency of the bubble formation as a function of the laser fluence, normalized by the size-dependent threshold fluence F_{thr}. For all the sizes analyzed, the efficiency displays a maximum for a fluence close to the fluence threshold. Beyond this maximum, the efficiency drops with the fluence. The maximal efficiency is found to decrease with the particle size, and remains below 41 percent.

The dependence of the maximal efficiency on the particle size may be understood qualitatively based on the relative role of the Kapitza resistance and heat diffusion in water. For the GNP sizes considered here, heat diffusion in the fluid is the longest process which controls the cooling kinetics of the nanoparticle with a relaxation time $\tau_{\mathrm{diff}} = R^2 m\rho_{\mathrm{liq}} C_v/\lambda$. On the other hand, nanobubble generation involves the vaporization time $t_{\mathrm{vap}} = \max(\tau_x, \tau_{\mathrm{int}}) = \tau_{\mathrm{int}}$ at the threshold fluence, where $\tau_{\mathrm{int}} = RC_{\mathrm{np}}/3G$ is the characteristic time introduced by the Kapitza resistance [13]. For small nanoparticles, the two relaxation times τ_{diff} and τ_{int} are comparable and the GNP is allowed to cool down and transfer the laser energy to the fluid before a nanobubble is produced. A significant part of this energy is used for the nanobubble growth and the efficiency is relatively high. For bigger GNPs, on the contrary, $\tau_{\mathrm{diff}} \gg \tau_{\mathrm{int}}$ so vaporization occurs before a significant amount of energy is transferred to the fluid. Due to the insulating role of the vapor layer the energy stored in the nanoparticle is not used for the bubble growth, resulting in a lower efficiency in the energy transfer for GNPs of larger radii.

The thermal boundary resistance also explains the efficiency drop as a function of the laser fluence. Close to the threshold fluence, the very large value of the

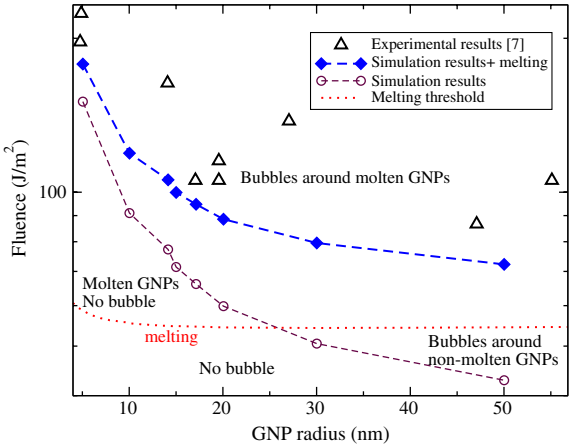

FIG. 5 (color online). Threshold fluence for GNP melting (red dotted line) compared with the explosive boiling threshold of water (squares). The melting threshold has been calculated based on a melting time $\tau_m = 30$ ps and a melting temperature $T_m = 1200$ K. The explosive boiling threshold has been calculated from thermohydrodynamics simulations without melting. With blue diamonds, we show the nanobubble threshold obtained by adding the enthalpy of melting $\Delta H_{\rm melt} = V_{\rm np} h_{\rm melt}$ (with $h_{\rm melt} = 1.24\ 10^9\,{\rm J/m^3}$ for gold) to the simulation results for the bubble-generation thresholds. The black triangles are experimental results from Ref. [7].

vaporization time induced by the Kapitza resistance allows an efficient transfer between the GNP and the nanobubble, as displayed in the inset of Fig. 4. However the vaporization time is a rapidly decreasing function of the fluence, as plotted in Fig. 3. When the fluence is increased, vaporization becomes faster and the energy transfer to water is strongly reduced, yielding to the drop in the efficiency.

Nanoparticle melting.—Another consequence of the slow vaporization kinetics close to the threshold is the possibility that the GNPs melt before any fluid phase change occurs. Femtosecond laser pulses induce heating of the GNP beyond gold's melting temperature ($T_m = 1200$ K) in a few picoseconds. Melting of the nanoparticle may then proceed, although this is not an instantaneous process. Note also that the particle may rapidly cool down below T_m and recrystallize, but nanoparticle recrystallization is a rather long process which occurs on nanosecond time scales [16]. Nanoparticle melting is indeed relevant because of the separation of time scales, with the melting time being smaller than vaporization times, which in turn are shorter than recrystallization times. Figure 5 displays a quantitative estimate of the melting threshold as a function of the nanoparticle size, estimated by solving a purely diffusive model [11] using a finite melting time $\tau_m = 30$ ps [16] and the GNP enthalpy of melting $\Delta H_{\rm melt}$. The calculated melting threshold accounts for heat diffusion in water, the gold-water thermal boundary resistance, and the kinetics of melting. We now compare this melting line with the onset of vaporization.

Thresholds.—Figure 5 shows the threshold fluence for bubble appearance, as found in our simulations. This line delimits two regions in the fluence/GNP radius space: above the threshold nanobubbles should appear, while below the energy supplied by the laser is not sufficient to drive vaporization. It is interesting to compare this vaporization line with the melting line discussed previously. For particle sizes smaller than 25 nm, the melting line falls in the region where nanobubbles cannot be generated. This implies that for these nanoparticle sizes, melting proceeds before vaporization and nanobubbles should form around molten nanoparticles. For particles having a radius larger than 25 nm, the melting line lies in the region where explosive vaporization sets in. For these particles, nanobubbles may be observed around unmolten nanoparticles, but Fig. 5 shows that the corresponding region is rather narrow.

We finally compare our predictions for the onset of vaporization with experimental data [7]. Figure 5 concludes that experimentally detected nanobubbles fall in the region where explosive boiling sets in, but they also fall in the region where GNP melting is relevant. The fluence thresholds obtained for nonmolten GNPs must be corrected to account for melting, and we have added in Fig. 5 the enthalpy of melting $\Delta H_{\rm melt}$ to our theoretical predictions. Interestingly, the new curve compares well with the experimental data; it delimits the region where nanobubbles are observed (above the curve), and the region where nanobubbles have never been reported (below the curve). This analysis shows the relative importance of nanoparticle melting.

Conclusion.—In summary, we probed theoretically the kinetics of nanobubble generation around metallic nanoparticles heated by a strong laser pulse. We emphasized the slow kinetics of vapor generation, especially in the vicinity of the nanobubble threshold. The slow kinetics explains the existence of an optimum in the energy efficiency of the vaporization process. We also concluded that experimentally nanobubbles should be observed around molten nanoparticles, as the long vaporization times allow melting to be quantitative. Considering this effect, our simulation data showed good agreement with experiments.

The authors thank F. Detcheverry for reading the manuscript and discussions.

*samy.merabia@univ-lyon1.fr

[1] D. Lapotko, Cancers **3**, 802 (2011).
[2] O. Neumann, A. S. Urban, J. Day, S. Lal, P. Norlander, and N. J. Halas, ACS Nano **7**, 42 (2013).
[3] L. R. Hirsch, R. J. Stafford, J. A. Bankson, S. R. Sershen, B. Rivera, R. E. Price, J. D. Hazle, N. J. Halas, and J. L. West, Proc. Natl. Acad. Sci. U.S.A. **100**, 13549 (2003).
[4] Z. Qin and J. C. Bischof, Chem. Soc. Rev. **41**, 1191 (2012).

[5] S. Hashimoto, D. Werner, and T. Uwada, J. Photochem. Photobiol. C **13**, 28 (2012).
[6] D. Wen, International Journal of Hyperthermia **25**, 533 (2009).
[7] A. Siems, S. A. L. Weber, J. Boneberg, and A. Plech, New J. Phys. **13**, 043018 (2011).
[8] E. Lukianova-Hleb, Y. Hu, L. Latterini, L. Tarpani, S. Lee, R. A. Drezek, J. H. Hafner, and D. O. Lapotko, ACS Nano **4**, 2109 (2010).
[9] R. Teshigawara and A. Onuki, Phys. Rev. E **82**, 021603 (2010).
[10] A. Onuki, Phys. Rev. E **75**, 036304 (2007).
[11] See Supplemental Material at http://link.aps.org/supplemental/10.1103/PhysRevLett.112.105701 for details regarding the numerical model, the Rayleigh-Plesset analysis, and the diffusive model which includes melting.
[12] The parameter t_p used here is larger than the pulse duration. We consider femtosecond pulses and the time t_p is the electron-phonon coupling time as described by Ref. [13], which determines the GNP phonon equilibration time: for times larger than t_p, the GNP may be considered uniformly heated. The electron interaction with the pulse prior to that coupling is not accounted for, as its characteristic time is a few times smaller than t_p. Other phenomena such as particle melting are not modeled here.
[13] V. Juve, M. Scardamaglia, P. Maioli, A. Crut, S. Merabia, L. Joly, N. Del Fatti, and F. Vallée, Phys. Rev. B **80**, 195406 (2009).
[14] Z. B. Ge, D. G. Cahill, and P. V. Braun, Phys. Rev. Lett. **96**, 186101 (2006).
[15] N. Shenogina, R. Godawat, P. Keblinski, and S. Garde, Phys. Rev. Lett. **102**, 156101 (2009).
[16] S. Inasawa, M. Sugiyama, S. Noda, and Y. Yamaguchi, J. Phys. Chem. B **110**, 3114 (2006).